Modeling the responsivity and self-emission of a double-beam Fourier-transform infrared interferometer

Jean-Marc Thériault

A modeling study aimed at characterizing the radiometric properties of a double-beam Fourier-transform infrared interferometer is presented. Measurements showed that the two responsivities associated with each interferometer channel are different in certain spectral regions. This anomaly was attributed to a dissymmetry between the optical transmissions of the two plates that form the beam splitter. This dissymmetry is primarily responsible for the instrument residual emission. A secondary cause of residual emission is attributed to the relative alignment of the two input optics. Both effects were taken into account in a model that gives the instrument residual emission in terms of the beam splitter temperature. Actual results indicate that in the 7–14-μm window the instrument residual emission can be modeled with an absolute radiometric error smaller than 0.5 K (blackbody at 290 K). The model was used to develop an automatic calibration procedure that yields radiance errors smaller than 0.05 $\mu W/cm^2$ sr cm^{-1} in the 7–14-μm band. The radiometric stability of the interferometer was analyzed.

OCIS codes: 010.0010, 300.6300, 280.1120, 260.3160, 230.1360, 010.1290, 220.2740.

1. Introduction

Fourier-transform infrared (FTIR) spectrometers are currently used in a variety of applications for the passive remote sensing of atmospheric species and pollutants.[1–9] In most of these applications they are used as spectral radiometers. In these cases the instrument must be calibrated radiometrically, and it is well known that such a calibration can be rather cumbersome. The main difficulty arises from the fact that the output signal contains parasite radiation that is mainly self-emission generated by the instrument. Consequently, a special calibration procedure that involves two reference measurements must be applied to obtain and correct for this self-emission term in addition to the usual responsivity parameter. In current FTIR spectrometers the self-emission is generally uncontrolled and variable in time. Thus the best way to acquire radiometrically accurate spectra is with frequent calibration measurements. The maximum accuracy is achieved when the two calibration measurements are updated for each target measurement, which increases the time required to generate a single calibrated spectrum by a factor of 3. This constraint of frequent calibration represents a serious burden, reducing the efficiency of FTIR instruments for real-time applications.

To make FTIR instruments more stable radiometrically and easier to calibrate, exploitation of the attributes of a double-beam FTIR interferometer adapted to suppress the instrument self-emission contributions is proposed. The expected goal is an FTIR interferometer that requires monitoring of only the beam splitter temperature in order to generate a calibrated spectrum in real time automatically. In this context the Defence Research Establishment Valcartier developed, in cooperation with Bomem, a double-beam system referred to as the compact atmospheric sounding interferometer (CATSI). The main application for this instrument is the remote detection and identification of chemical vapors.[10–12]

In the design phase of the CATSI instrument, special care was taken to respect the symmetry criteria that permit self-emission suppression. The strategy was to make the two interferometer channels as identical as optically possible. In particular, a design for a symmetrical configuration for the beam splitter assembly was needed. The one selected for CATSI is made essentially of two plates separated by a thin air layer. In principle, with such a beam splitter configuration the radiation made up mainly of the self-

The author is with the Defence Research Establishment Valcartier, 2459 Pie XI Boulevard, North Val-Belair, Quebec G3J 1X5, Canada. His email address is jean-marc.theriault@drev.dnd.ca.

Received 5 June 1998; revised manuscript received 24 September 1998.

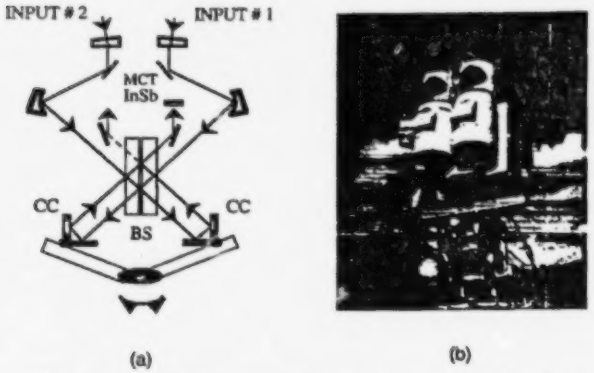

Fig. 1. (a) Optical diagram and (b) picture of the CATSI.

emission from one plate exactly cancels the self-emission from the other plate, because they are 180° out of phase. Although the level of suppression obtained with this configuration of CATSI is quite significant, some limitations in the suppression level were observed in certain spectral regions, including a severe anomaly in the region below 700 cm^{-1}. After analysis it was found that these limitations are due primarily to an unexpected dissymmetry between the transmissions of the two plates that form the beam splitter. As a consequence, the two responsivities associated with each interferometer channel are different, and the resulting imbalance is responsible for the instrument residual emission. In this paper we present a modeling study aimed at characterizing the observed responsivity and self-emission of the CATSI system. The modeling system is then used to develop an automatic calibration procedure that is based on the beam splitter temperature.

2. Compact Atmospheric Sounding Interferometer

The technique of dual-beam interferometry was first suggested by Fellgett[13] and subsequently exploited in various laboratory and astrophysical measurements.[14] For example, Vanasse and co-workers[14–16] developed a background suppression technique that is based on the optical subtraction capability of a double-beam FTIR interferometer operating in the 3–5-μm band. Another example is a dual-beam interferometer for optical difference measurements.[17] It was designed for performing sample reflectivity and absorption measurements in the 10–400-cm^{-1} band. Additional references on double-beam interferometers can be found in Ref. 14. By comparison with other FTIR instruments, the unique feature of the CATSI system is its optimization for suppressing the instrument self-emission by optical subtraction.

Essentially, the CATSI system is made of two identical 4-in.-diameter Newtonian telescopes optically coupled to the dual-beam interferometer. Figure 1 summarizes the optical design in the left-hand panel and shows the instrument mounted on a tripod in the right-hand panel. An important effort was deployed to respect symmetry criteria. Actually, half of the instrument is designed to be a mirror reflection of the other half, with the beam splitter center as a reference plane. The CATSI system allows for measurements of spectra according to the following specifications: scene fields of view from 4 to 11 mrad, spectral coverage from 3 to 18 μm, and a spectral resolution from 1 to 128 cm^{-1}. A flat plate mirror placed in front of each telescope can be rotated to the selected scene. The pointing capability of this scene mirror allows for azimuth measurements from 0° to 180°. After reflection on the scene mirror the input beam is focused with the Newtonian telescope at the entrance of the interferometer and is then reflected with an off-axis parabolic mirror to produce a collimated beam of proper diameter in front of the beam splitter.

A double-pendulum scanning mechanism controls the periodic displacement of the two corner reflectors (CC) that generate the interferogram. The beam splitter consists of a thin air gap squeezed between two ZnSe substrates with antireflection (AR) coatings on their external faces. A thermistor attached to the beam splitter holder provides continuous monitoring of the beam splitter temperature. This beam splitter temperature is used to evaluate the radiometric parameters needed for an automatic calibration. Of the two output channels only one is used at this moment. This output module contains parabolic and condensing mirrors that focus the beam onto a sandwich MCT–InSb detector (1 mm) mounted on a microcooler. The MCT element is optimized for the 6–18-μm spectral region, whereas the InSb element is optimized for the 2–5-μm region. Two CCD cameras mounted on the top of the two telescope modules can be used to aim and view the scenes under consideration. With this instrument two scenes that come from adjacent fields of view are combined optically at the detector level. The overall system weighs approximately 40 lb (18 kg) with a linear size of 13 in. (33 cm).

3. Double-Beam Fourier-Transform Infrared Interferometer: Radiometric Attributes

As seen in Fig. 1(a) the reflected beams from corner reflectors are offset laterally from the incident beams. This is an advantage, because it permits decoupling input and output channels as opposed to the standard single-beam interferometer. This attribute makes it possible to adjust the self-emission from each input port independently without affecting the output optics, in any way which is not possible with the single-beam configuration. The strategy also consisted of designing the double-beam interferometer such that the two self-emission terms from each input port could be made equal in intensity and 180° out of phase thus leading to a theoretically perfect cancellation.

In such a design there are two main factors that limit the accuracy of the optical suppression. The first factor is related to the optical configuration of the two input ports (mirrors and windows). These two inputs must be as symmetric as possible to ensure the same beam attenuation and consequently

the same emission from both ports. For example, if the absorption of a mirror (or lens) from input 1 is greater than its counterpart from input 2, then the resulting imbalance corresponds to a greater emission from input 1. In practice it is relatively easy to satisfy this symmetry requirement with a proper mechanical design and with the use of identical optical components in each input port. The second limiting factor is related to the IR emission from the beam splitter. Of these two factors the latter is usually the most important. The effect of beam splitter self-emission is an important issue that has been observed in many types of FTIR instrument. For example, the mechanism responsible for the dual-phase response of the High-Resolution Interferometer Sounder was identified as emission from the interferometer beam splitter.[18] Another example is the phase anomaly of the Michelson Interferometer for Passive Atmospheric Sounding (MIPAS), which was explained and corrected for by taking into account the beam splitter emission.[19,20] A simple method for computing the beam-splitter layer emission of the FTIR interferometer is proposed in a companion paper.[21]

The following equations serve to establish the expected characteristics of the CATSI instrument. For a FTIR spectrometer based on a double-input port interferometer the total signal $\mathbf{S}$ represents the sum of two individual complex raw spectra, $\mathbf{E}_1$ and $\mathbf{E}_2$, associated with each input. If input 1 and input 2 aim at target sources of radiance L_1 and L_2, respectively, the resulting raw spectrum is given by

$$\mathbf{S} = \mathbf{E}_1 + \mathbf{E}_2 + \mathbf{E}_{\text{layer}}, \tag{1}$$

with

$$\mathbf{E}_1 = \mathbf{K}_1(L_1 + \mathbf{SE}_{\text{in1}}), \tag{2}$$

$$\mathbf{E}_2 = \mathbf{K}_2(L_2 + \mathbf{SE}_{\text{in2}}), \tag{3}$$

where $\mathbf{K}_1$ and $\mathbf{K}_2$ are defined as the responsivities associated with input 1 and input 2, respectively. The terms $\mathbf{SE}_{\text{in1}}$ and $\mathbf{SE}_{\text{in2}}$ correspond to the self-emissions associated with input 1 and input 2, respectively. Each term includes the self-emissions from the various optical components of the corresponding input. It is important to note that the self-emission from each ZnSe plate that makes up the beam splitter assembly is also included in these terms. For example, with reference to Fig. 1(a), the self-emission contribution from the right-hand ZnSe plate is included in the term $\mathbf{SE}_{\text{in1}}$, whereas the self-emission from the left-hand plate is included in the term $\mathbf{SE}_{\text{in2}}$. For practical reasons it appeared convenient to group into the $\mathbf{SE}_{\text{in1}}$ and $\mathbf{SE}_{\text{in2}}$ terms the self-emission of any input component that had a symmetric counterpart in the other input (e.g., mirrors and plates). The only component of self-emission that cannot be included directly in one of these two terms is the one from the splitting layer. It is defined here as $\mathbf{E}_{\text{layer}}$ and is taken into account separately in Eq. (1). However, as discussed in Ref. 21, $\mathbf{E}_{\text{layer}} = 0$ for the CATSI system, because the emission or scattering of a thin layer of air is assumed to be negligible. For this reason $\mathbf{E}_{\text{layer}}$ is neglected in the following equations.

To study the radiometric symmetry or balance of the dual-beam interferometer it is advantageous to proceed by analogy with the single-beam calibration approach. In the particular case in which the calibration is performed on input 2 (arbitrary) while the source L_1 is fixed for the three measurements (target and two references) the corresponding raw spectrum can be written as

$$\mathbf{S} = \mathbf{K}_2(L_2 + \mathbf{O}_2), \tag{4}$$

with

$$\mathbf{O}_2 = \left(\mathbf{SE}_{\text{in2}} + \frac{\mathbf{K}_1}{\mathbf{K}_2}L_1 + \frac{\mathbf{K}_1}{\mathbf{K}_2}\mathbf{SE}_{\text{in1}}\right), \tag{5}$$

where the two parameters required for the radiometric calibration are defined as

$$\mathbf{K}_2 = \frac{\mathbf{S}_{\text{hot}} - \mathbf{S}_{\text{amb}}}{B_{\text{hot}} - B_{\text{amb}}}, \tag{6}$$

$$\mathbf{O}_2 = \frac{\mathbf{S}_{\text{amb}}B_{\text{hot}} - \mathbf{S}_{\text{hot}}B_{\text{amb}}}{\mathbf{S}_{\text{hot}} - \mathbf{S}_{\text{amb}}}. \tag{7}$$

Note that the source L_1 acts as a part of the instrument offset. Equations (4) and (5) link the complex raw spectrum $\mathbf{S}$ to the target spectrum L_2 (the one to be evaluated), taking into account the characteristics of the double-beam interferometer, which are the complex spectral responsivity $\mathbf{K}_2$ and the complex spectral offset $\mathbf{O}_2$ associated with channel 2. The method used to obtain these two calibration parameters is the one proposed by Revercomb *et al.*[18] It is often referred to as the two-temperature calibration method. With this method, two reference blackbodies of known radiance, B_{hot} and B_{amb}, and their corresponding raw spectrum, $\mathbf{S}_{\text{hot}}$ and $\mathbf{S}_{\text{amb}}$, are required for solving the two unknowns $\mathbf{K}_2$ and $\mathbf{O}_2$.

When applied to a properly designed double-beam interferometer this radiometric calibration can be simplified. From Eq. (5) it can be seen that the spectral offset $\mathbf{O}_2$ associated with channel 2 can be minimized by the fulfillment of two conditions: (i) the condition of balanced responsivities [$\mathbf{K}_1 = -\mathbf{K}_2 = \mathbf{K}_2 \exp(i\pi)$] and (ii) the condition of balanced emissions ($\mathbf{SE}_{\text{in1}} = \mathbf{SE}_{\text{in2}}$). When these two conditions are applied the resulting raw spectrum [Eqs. (4) and (5)] is reduced to

$$\mathbf{S} = \mathbf{K}_2(L_2 - L_1). \tag{8}$$

In this form Eq. (8) does not contain any self-emission terms from the instrument. The resulting raw spectrum $\mathbf{S}$ is directly proportional to the difference between the two source radiances $L_2 - L_1$. Consequently, for single-beam operations this instrument requires the use of a fixed reference source of known radiance ($L_1 = L_{\text{ref}}$) attached to the first input port. This reference can be a simple black plate with a

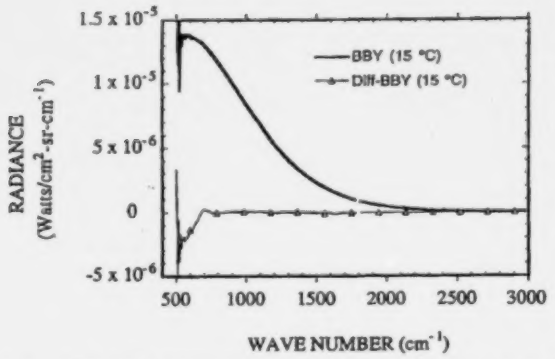

Fig. 2. Calibrated measurement of a blackbody (BBY) at 15 °C (upper curve) and the resulting difference when the two ports are used.

thermocouple for monitoring the plate temperature, which allows for the computation of the Planck radiance L_1.

This approach considerably simplifies the radiometric calibration in which in principle only one reference measurement is needed to evaluate the spectral responsivity $\mathbf{K}_2$ of the instrument (no offset). Moreover, as discussed below in Section 5, the responsivity of the CATSI instrument is highly correlated to the beam splitter temperature. Consequently, prestored coefficients can be used to model the temperature dependence of the responsivity $\mathbf{K}_2(T_{BS})$, thus allowing for its evaluation in real time. In these conditions the calibrated radiance is given by

$$L_2 = \left(\frac{\mathbf{S}}{\mathbf{K}_2(T_{BS})} + L_1\right). \tag{9}$$

The net result is an FTIR spectrometer that requires only monitoring of the beam splitter temperature and a flat plate to generate, in real time, a calibrated spectrum according to Eq. (9). Note that in a practical design the casing of the instrument can be made to integrate the flat plate and the beam splitter onto the same mount such that $T_{BS} = T_{ref}$, which results in only one temperature monitoring to obtain the calibrated spectrum.

A final advantage of the CATSI design is for the differential detection of weak IR signatures against large spectral backgrounds.[10] Because the subtraction is instantaneously performed optically, the calibrated differential ($\delta L = L_2 - L_1$) can be evaluated in real time with

$$\delta L = \frac{\mathbf{S}}{\mathbf{K}_2(T_{BS})}. \tag{10}$$

Equations (9) and (10) represent the ideal case, i.e., a perfectly balanced double-beam interferometer. However, in practice it was found that with the actual CATSI system there are some limitations. As an example, Fig. 2 shows the measured radiance of a blackbody at 15 °C (upper curve) and the resulting difference when the two input ports view the same blackbody (15 °C). The suppression effect is obvious. However, the resulting difference (bottom curve) is not exactly zero. Above 700 cm^{-1} the residual is of the order of a few percent, and in the 500–700-cm^{-1} region the spectral residual is of the order of 15%. After investigation we came to the conclusion that these residuals arise from the limited performance of the beam splitter. An undesired dissymmetry between the optical properties of the two ZnSe substrates that form the beam splitter was found. This is due in part to nonidentical antireflection coatings present on the external face of each substrate and in part to a difference between the transmission associated with each substrate. Both effects introduce a dissymmetry in the self-emission and the attenuation associated with each port. A useful model that predicts the instrument residual emission in terms of the optical characteristics of both beam splitter substrates is presented in Appendix A.

4. Modeling the Instrument Residual

In many applications the required level of radiometric error is of the order of or smaller than 0.01–0.02 $\mu W/cm^2$ sr cm^{-1}. An example of such an application is the retrieval of atmospheric gases from the downwelling spectral radiance. In this case the radiance level generated by gases such as CO_2, N_2O, chlorofluorocarbons, and HNO_3 in the 8–12-μm region can be as low as 0.04–0.5 $\mu W/cm^2$ sr cm^{-1} for cold sky observations in the winter. To obtain this level of accuracy with the actual CATSI system the instrument residual emission must be taken into account. Moreover, to satisfy the objective of a real-time (or automatic) calibration that is based on beam splitter temperature, it is necessary to model the residual accordingly. In this context the equations for obtaining the radiance [Eq. (9)] and the differential [Eq. (10)] must be extended to include an instrument residual emission $\mathbf{re}_2$ defined such that

$$L_2 = \frac{\mathbf{S}}{\mathbf{K}_2(T_{BS})} + L_1 - \mathbf{re}_2(T_{BS}) \tag{11}$$

or, for the differential operation mode,

$$\delta L = \frac{\mathbf{S}}{\mathbf{K}_2(T_{BS})} - \mathbf{re}_2(T_{BS}). \tag{12}$$

To evaluate the instrument residual emission $\mathbf{re}_2$ from the substrates dissymmetry, we use the results established in Eqs. (A15) and (A16), where it was found that the raw spectrum associated with the self-emission of each substrate is given by

$$\text{raw spec}(\varepsilon_1) = \mathbf{K}_1 \frac{(1 - T_{c1}T_{s1})}{T_{c1}T_{s1}} B_s, \tag{13}$$

$$\text{raw spec}(\varepsilon_2) = \mathbf{K}_2 \frac{(1 - T_{c2}T_{s2})}{T_{c2}T_{s2}} B_s \tag{14}$$

for substrate 1 [Eq. (A15)] and substrate 2 [Eq. (A16)], respectively. Note that T_{c1}, T_{c2} and T_{s1}, T_{s2}

represent the transmittances of the associated AR coatings and substrates, respectively. B_s is the Planck radiance related to the substrate temperature. In this case, if input 1 and input 2 look at target sources of radiance L_1 and L_2, respectively, the resulting raw spectrum is given by

$$\mathbf{S} = \mathbf{E}_1 + \mathbf{E}_2, \tag{15}$$

with

$$\mathbf{E}_1 = \mathbf{K}_1\left[L_1 + \frac{(1 - T_{c1}T_{s1})}{T_{c1}T_{s1}}B_s\right], \tag{16}$$

$$\mathbf{E}_2 = \mathbf{K}_2\left[L_2 + \frac{(1 - T_{c2}T_{s2})}{T_{c2}T_{s2}}B_s\right]. \tag{17}$$

To obtain these two equations, we make the hypothesis (for the moment) that the main source of unsuppressed self-emission comes from the beam splitter substrates alone, assuming that other self-emission contributions from the two input optics cancel out. Rewriting Eq. (17) to obtain the raw spectrum in terms of the instrument residual emission $\mathbf{re}_2$ yields

$$\mathbf{S} = \mathbf{K}_2[L_2 - L_1 + \mathbf{re}_2] \tag{18}$$

or

$$\mathbf{S} = \mathbf{K}_2\left[L_2 - L_1 + \left(1 + \frac{\mathbf{K}_1}{\mathbf{K}_2}\right)L_1 + \frac{\mathbf{K}_1}{\mathbf{K}_2}\frac{(1 - T_{c1}T_{s1})}{T_{c1}T_{s1}}B_s + \frac{(1 - T_{c2}T_{s2})}{T_{c2}T_{s2}}B_s\right]. \tag{19}$$

Further simplifications result from use of the relations established in Eqs. (A10) and (A11), which show that the ratio of the two responsivities is given by

$$\frac{\mathbf{K}_1}{\mathbf{K}_2} = -\frac{T_{c1}T_{s1}}{T_{c2}T_{s2}}, \tag{20}$$

which, after insertion into Eq. (19), yields

$$\mathbf{re}_2 = \left(1 + \frac{\mathbf{K}_1}{\mathbf{K}_2}\right)[L_1 - B_s]. \tag{21}$$

Equation (21) is a simple and useful relation. It gives the spectral residual of a double-beam interferometer with an optical dissymmetry between the two beam splitter substrates. This dissymmetry has the consequence that in certain spectral regions the responsivities $\mathbf{K}_1$ and $\mathbf{K}_2$ are not fully balanced. This is shown in Fig. 3, where the measured module and phase of the responsivity ratio are reported for the CATSI system (without telescopes and input windows). Above 800 cm^{-1} the instrument behaves as expected. The module ratio and the phase difference are approximately 1 and 180°, respectively. In this case Eq. (21) shows that the residual $\mathbf{re}_2$ should be near zero ($\mathbf{K}_1 = -\mathbf{K}_2$), thus yielding an efficient suppression. However, below 800 cm^{-1} the module ratio changes rapidly, peaking near 700 cm^{-1} at a value of 1.05 and decreasing down to a value of 0.2

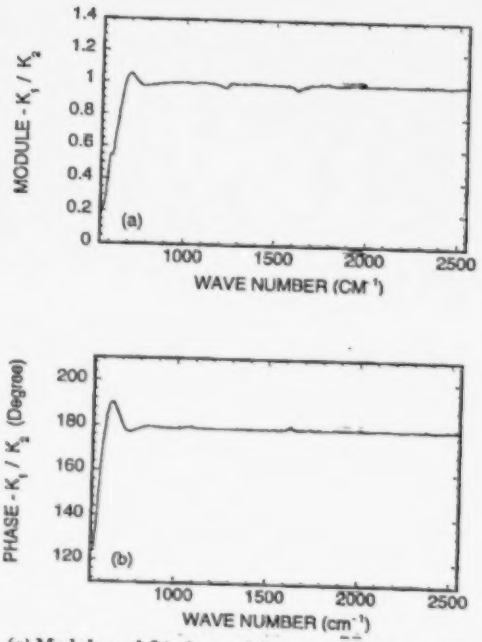

Fig. 3. (a) Module and (b) phase of the responsivity ratio $\mathbf{K}_1/\mathbf{K}_2$ of the CATSI system (without telescopes and input windows).

near 550 cm^{-1}. Such a dissymmetry in substrate absorption (or transmission) induces an important imbalance in the beam splitter self-emission, thus resulting in a large instrument residual emission ($\mathbf{re}_2$).

Also interesting in this region below 800 cm^{-1} is that the phase difference between the two responsivities oscillates between approximately 125° and 190° [Fig. 3(b)]. This seems to be in opposition to the result established in Eqs. (A10) and (A11), which indicates that the phase difference between the two responsivities is always 180°. Actually, the 180° phase difference is exact for a single polarization axis (s or p) of the beam splitter. As discussed in Appendix A, for the general case of mixed polarization (or unpolarized) that corresponds to our measurements (Fig. 3), effective phase differences other than 180° can occur without destruction of the applicability of Eq. (21).

A validation of Eq. (21) is presented in Fig. 4, where measured and predicted instrument residual emissions ($\mathbf{re}_2$) are compared. The measured residual emission is obtained directly by application of the two-temperature calibration method [Eqs. (6) and (7)]. The predicted residual emission [Eq. (21)] is calculated with the responsivity ratio (Fig. 3), the measured beam splitter temperature, and the radiance of the source L_1 as inputs. Note that the beam splitter temperature is monitored continuously by a thermistor attached to the beam splitter holder. For cases presented in Fig. 4 the beam splitter temperature was stable at 35.8 °C, for which three different temperatures (5.9, 35.1, and 44.8 °C) were selected for the source L_1 (blackbody). The behavior of the

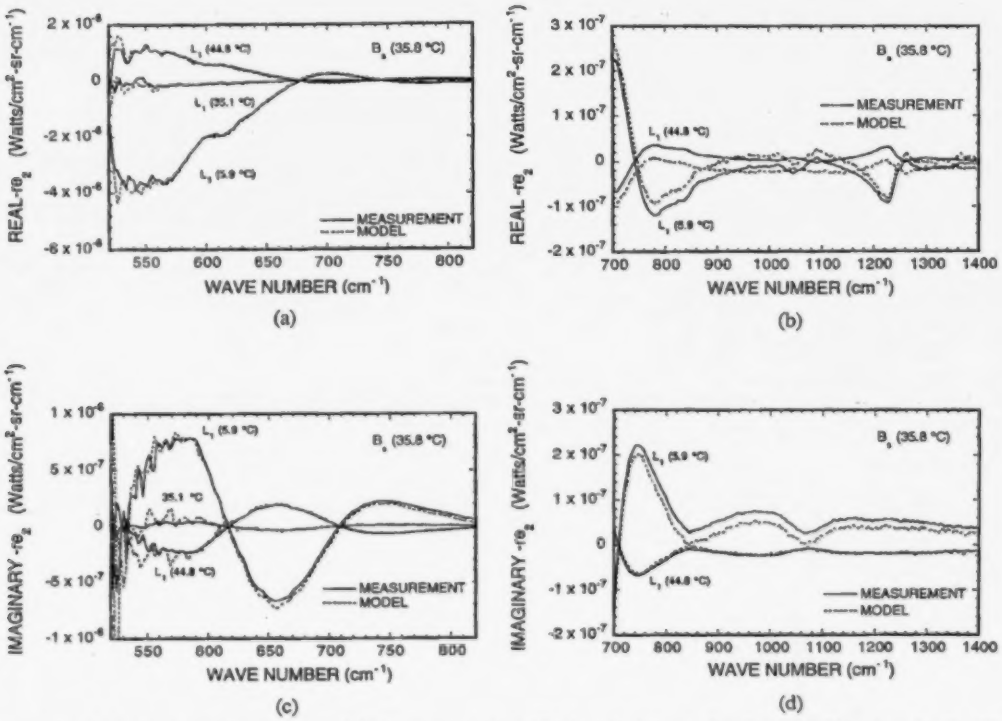

Fig. 4. Comparison of the measured and the modeled instrument residual emission $\mathbf{re}_2$ for the CATSI system in the 500–1400-cm^{-1} spectral region. Here (a) and (b) correspond to the real part, whereas (c) and (d) correspond to the imaginary part of $\mathbf{re}_2$. The 1800–2800-cm^{-1} spectral region shows the same level of agreement.

residual strongly depends on the temperature difference between the source and the beam splitter (through $L_1 - B_s$). As predicated by Eq. (21), if there is no radiance contrast between the source and the beam splitter ($L_1 - B_s \sim 0$), then the residual should be zero. This is observed in Figs. 4(a) and 4(c) for the case in which the source temperature (35.1 °C) is very close to that of the beam splitter (35.8 °C). For a negative temperature difference (i.e., 5.9–35.8 °C), Eq. (21) predicts a negative real part [Fig. 4(a)] and a positive imaginary part [Fig. 4(c)] for the residual in the 550–650-cm^{-1} region. This is also observed in the measurements. The reverse situation happens for a positive temperature difference (i.e., 44.8–35.8 °C), which yields a positive real part and a negative imaginary part of the residual in this spectral region. Overall, the measured behavior of the instrument residual emission is quite well modeled by Eq. (21). As seen in Figs. 4(b) and 4(d), typical differences between measured and predicted $\mathbf{re}_2$ are usually smaller than 4×10^{-8} W/cm^2 sr cm^{-1}, which represents, for comparison, a 0.5% of the radiance of a blackbody at 15 °C. Note that for clarity the case corresponding to a source temperature of 35.1 °C in Figs. 4(b) and 4(d) was removed. In this case the measured and modeled curves are almost superimposed to the zero axis in the 700–1400-cm^{-1} range with differences smaller than 2×10^{-8} W/cm^2 sr cm^{-1}. Many comparisons indicate the same level of accuracy with other source and beam splitter temperatures and also for the mid-IR region.

5. Automatic Calibration

A common strategy for obtaining radiometric accuracy with standard FTIR interferometers is to perform frequent calibrations to compensate for the thermally induced variations of instrument residual emission and responsivity. For the double-beam interferometer of the CATSI system it was shown that one can monitor the variation of the instrument residual emission $\mathbf{re}_2$ by monitoring the beam splitter temperature, which represents a first step toward an automatic calibration. The second step is modeling the responsivity in terms of beam splitter temperature. Thus if both calibration parameters, $\mathbf{re}_2$ and $\mathbf{K}_2$, are estimated from the monitored beam splitter temperature, then an automatic (real-time) calibration can be achieved.

In the model of $\mathbf{re}_2$ discussed in Section 5, Eq. (21) was validated with measurements made with a simplified version of the CATSI system, i.e., without the two input telescopes and input windows. This simplification was justified by the need to isolate clearly the beam splitter contribution from other contributions included in the responsivity and self-emission. Actually, to model the instrument residual emission of the complete CATSI instrument [Fig. 1(b)], the

form of Eq. (21) must be extended slightly to take into account the residual imbalance caused by the relative alignment, vignetting, and extinction of the two input telescopes (and windows). These effects can be taken into account by the introduction of the related transmission and emission terms at the level of Eq. (19). In this case the resulting instrument residual emission expression for the complete CATSI system can be written as

$$\mathbf{re}_2 = \left(1 + \frac{\mathbf{K}_1}{\mathbf{K}_2}\right)[L_1 - B_s] + (\alpha K_2^{-1} + \gamma)B_s, \quad (22)$$

where two new spectral coefficients γ and α are introduced. Each coefficient is related analytically to a finite number of terms that characterize the two telescopes and windows. Note that the advantage of this form is that the intervening terms can be taken into account through two spectral coefficients (γ and α) to be calibrated experimentally. The γ coefficients handle the unbalanced emissions from the two input telescopes (and windows). The temperature of the telescopes is assumed to be equal to the beam splitter temperature (B_s). Usually, the telescope temperature is approximately 5 °C below that of the beam splitter. Such a temperature difference has a negligible impact on Eq. (22). The second spectral coefficient α is introduced to take into account a slight temperature dependence (through $\mathbf{K}_2$) of unbalanced transmittances caused by relative misalignments between the two input telescopes. Note that if the two telescopes (and windows) were optically identical and perfectly coaligned then their emission contributions would be perfectly balanced, yielding $\gamma = 0$ and $\alpha = 0$.

To evaluate the accuracy of Eq. (22) in modeling the instrument residual emission of the CATSI system, a series of 20 calibrated measurements was made for a variety of source (L_1) and beam splitter (B_s) temperature combinations. Both telescopes were fixed on the same source ($L_2 = L_1$). The two-temperature calibration method was applied to evaluate the measured instrument residual emission. Two types of source were used to cover a wide range of temperatures. The first one was a bath of liquid nitrogen. The second one was a flat plate blackbody for which the temperature was selected from 5 to 50 °C. The selection of beam splitter temperatures was achieved with measurements performed at different steps of the instrument warm-up process. This provided a series of beam splitter temperatures varying from approximately 290 to 309 K, which covers the expected range of operation of the CATSI system.

From this set of measurements the three spectral coefficients $\mathbf{K}_1/\mathbf{K}_2$, γ, and α that best fit Eq. (22) were evaluated. Note that it was verified experimentally that the ratio $\mathbf{K}_1/\mathbf{K}_2$ is practically independent of the beam splitter temperature. To verify the consistency of the fit, these coefficients ($\mathbf{K}_1/\mathbf{K}_2$, γ, and α) were used to predict the instrument residual emission for each of the measurements (20 cases). The reason for this is to verify the efficiency of modeling the instrument residual emission and then remove it from the actual value. The result is summarized in Fig. 5. The rms value that covers the 20 measured residuals (upper curve) is compared with the rms value obtained after subtraction of the predicted $\mathbf{re}_2$. Both curves are expressed in brightness temperature error referenced to a blackbody at 290 K. As seen, the modeling is quite accurate, thus reducing the residual by a factor of approximately 4 in the IR window from 700 to 1400 cm^{-1} (7–14 μm). This result suggests that the instrument residual emission of the complete CATSI system can be modeled with an error smaller than 0.5 °C in this spectral region.

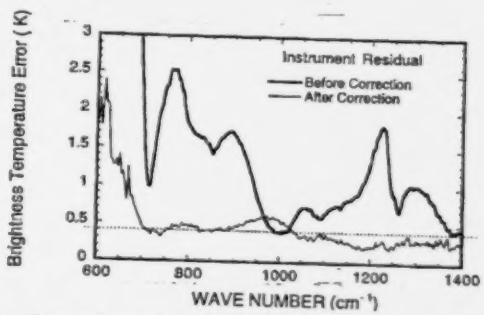

Fig. 5. Comparison of the measured rms value of instrument residuals (upper curve) with the rms value obtained after subtraction with the predicted residual (see text).

The last step for achieving an automatic calibration is the modeling of the responsivity ($\mathbf{K}_2$) in terms of beam splitter temperature. This is required for computing the radiance [Eq. (11) or Eq. (12)] and also the instrument residual emission [Eq. (22)]. This modeling can be rather complex if we take into account the temperature dependence of each hardware element (optical and electrical) that affects the responsivity. To avoid this complexity the following empirical approach was used. On the basis of the two-temperature calibration method a series of spectral responsivities for the selected range of beam splitter temperatures was measured. These spectra were assembled in the form of a look-up table and tagged with their respective beam splitter temperatures. Then the responsivity corresponding to a specific beam splitter temperature is found by a linear interpolation performed with the two closest results of the look-up table. As an example, Fig. 6 summarizes the dependence of $\mathbf{K}_2^{-1}$ for the 800–1200-cm^{-1} spectral region and for some of the temperatures that appear in the lookup table. As seen, the temperature dependence of $\mathbf{K}_2^{-1}$ is quite significant with a continuous variation of approximately 15% across the expected range of beam splitter temperatures. The spectrum corresponding to a temperature of 304.7 K (16 May 1998) was recorded 11 days after the others. This illustrates the high level of reproducibility over a relatively long period of time.

As a preliminary step for developing an operational procedure for an automatic calibration in real time an

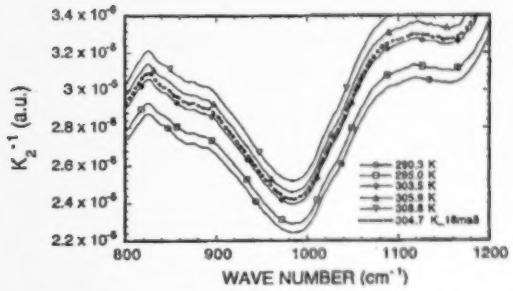

Fig. 6. Dependence of the $\mathbf{K}_2^{-1}$ parameter (inverse responsivity) to different beam splitter temperatures. The spectrum corresponding to 304.7 K was recorded 11 days after the others (see text).

additional calibration function was implemented into the processing package of the CATSI system. This function generates two calibrated spectra for the same target. One is derived from the usual two-temperature calibration method, which is considered to be the reference (truth), and the second is obtained by the automatic calibration that is based on monitoring the beam splitter temperature. The interest of this is to evaluate the long-term reproducibility of the $\mathbf{K}_2$ temperature dependence and also the temporal stability of the spectral coefficients ($\mathbf{K}_1/\mathbf{K}_2$, γ, and α) reported above. In addition, the compilation of these pairs of calibrated spectra over a long period of time serves to establish the robustness of the automatic calibration approach.

An example of comparison results is given in Fig. 7. This corresponds to a routine measurement performed to acquire the radiance spectrum of a mountain situated at approximately 10 km (one type of background). This measurement was recorded approximately two months after the characterization phase of the instrument (determination of $\mathbf{K}_1/\mathbf{K}_2$, γ, α, and a lookup table for $\mathbf{K}_2$). As seen, even after a two-month period the stability is such that the automatic calibration yields a spectral radiance quite similar to the actual one (two-temperature calibration method) with differences smaller than 5×10^{-8} W/cm^2 sr cm^{-1} in the 700–1400-cm^{-1} (7–14-μm) spectral region. This high level of stability was expected from a previous statistical study.[11] It was found from the analysis of more than 500 field spectra that the temporal drift of the responsivity and the offset of CATSI can be correlated to the instrument temperature to within an error of 2% over a period of eight days. Figure 7 also shows a more important discrepancy (2%–3%) in the region below 700 cm^{-1}. This indicates that the spectral coefficients ($\mathbf{K}_1/\mathbf{K}_2$, γ, α, and a look-up table for $\mathbf{K}_2$) for the automatic calibration procedure appears less stable in regions of strong beam splitter dissymmetry. The long-term stability will be addressed specifically in future studies when more data become available.

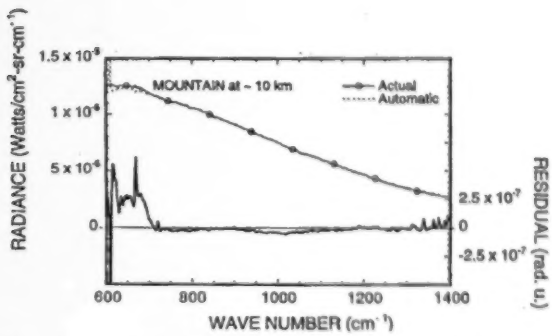

Fig. 7. Comparison of the two calibration methods used to obtain the spectral radiance of a forested mountain (background) situated at 10 km. The actual curve refers to the two-temperature calibration method, and the automatic calibration is based on the beam splitter temperature. The bottom curve (right scale) represents the difference between the two.

6. Conclusion

The concept of a balanced double-input beam interferometer to suppress the instrument self-emission contributions appears promising. Technically, the suppression is achieved when the two responsivities associated with each interferometer channel are equal in magnitude and opposite in phase. The CATSI system was developed to exploit this concept. The level of suppression obtained with the actual system is quite significant. However, some limitations in the suppression level were observed in certain spectral regions, including a severe anomaly in the regions below 700 cm^{-1}.

The modeling study presented in this paper elucidates these suppression limitations. Two causes of instrument residual emission were identified. The primary cause is due to an unexpected dissymmetry between the transmissions of the two substrates that form the beam splitter. As a consequence, the two responsivities associated with each interferometer channel are different [Eq. (20)] and the resulting imbalance is responsible for the instrument residual emission [Eq. (21)]. The secondary cause of instrument residual emission is attributed to limitations in the relative alignment of the two input optics of the CATSI system. Both the beam splitter effect and the alignment effect have been accounted for in a simple empirical model [Eq. (22)] that gives the instrument residual emission in terms of the beam splitter temperature. Experimental measurements performed for different beam splitter temperatures agree quite well with values predicted by the model. Actual results indicate that in the 7–14-μm window the instrument residual emission of the complete CATSI system can be modeled with an absolute error equivalent to 0.5 K for a blackbody at 290 K. Better accuracy can be obtained with a more precise evaluation of the prestored coefficients in the model.

The second aspect of this study has addressed the feasibility of an automatic calibration procedure. In this procedure the beam splitter temperature is used as input into a predictor model that corrects for the thermal variations of the instrument responsivity

and residual. Many measurements of CATSI responsivity indicate a high correlation with the beam splitter temperature. The responsivity changes by approximately 15% over the expected range of beam splitter temperatures (289–310 K) with a reproducibility estimated to be of the order of 1% over a period of several weeks. Typical results obtained two months after the determination of the prestored spectral coefficients indicate that the automatic calibration yields calibrated spectra quite similar to the actual ones with differences smaller than 0.05 $\mu W/cm^2\ sr\ cm^{-1}$ in the 7–14-μm window. This illustrates the high radiometric stability and reproducibility of the CATSI system over a long period of time. However, the calibration that is based on beam splitter temperature is not a permanent solution. The CATSI instrument has to be moved and operated in a variety of unstable and dusty environments. Consequently, there is a long-term drift of the calibration parameters associated with alignment and instrument aging. Therefore the two-temperature calibration method is being adapted to integrate the results of the modeling. With this adaptation the two-reference measurements will serve to update (on request) the prestored spectral coefficients of the predictor model, and the actual instrument responsivity and residual will be evaluated on the basis of the beam splitter temperature and the latest set of spectral coefficients.

Appendix A: Modeling Beam Splitter Self-Emission

The beam splitter configuration selected for the CATSI system is made of an optically thin layer of air squeezed between two thick ZnSe substrates properly covered with AR coatings on their external faces. The observed performances with the system suggested an optical dissymmetry between the two ZnSe substrates that form the beam splitter. To model this dissymmetry, expressions were developed for the responsivities $\mathbf{K}_1$ and $\mathbf{K}_2$ and for the beam splitter emission with some basic properties of optical thin films.[22]

Let us assume that the two substrates and their AR coatings might be optically different to simulate a possible mismatch. The ray tracings in Fig. 8 indicate that the output amplitudes ($\mathbf{A}_1$ and $\mathbf{A}_2$) for beams of unit amplitudes incident on input 1 and input 2 are given by

$$\mathbf{A}_1 = (\mathbf{t}_{c1}{}^3\mathbf{t}_{s1}{}^3\mathbf{r}\mathbf{t}\mathbf{t}_{c2}\mathbf{t}_{s2}) + [\mathbf{t}_{c1}\mathbf{t}_{s1}\mathbf{t}\mathbf{r}\mathbf{t}_{c2}{}^3\mathbf{t}_{s2}{}^3 \exp(i\phi)], \quad \text{(A1)}$$

$$\mathbf{A}_2 = (\mathbf{t}_{c2}{}^2\mathbf{t}_{s2}{}^2\mathbf{t}^2\mathbf{t}_{c1}{}^2\mathbf{t}_{s1}{}^2) + [\mathbf{t}_{c2}{}^4\mathbf{t}_{s2}{}^4\mathbf{r}^2 \exp(i\phi)], \quad \text{(A2)}$$

where $\mathbf{r}$ and $\mathbf{t}$ represent the amplitude reflection and transmission, respectively, of the thin air layer and $\phi = 2\pi x$ is the phase difference between the two interfering beams. The variables $\mathbf{t}_{c1}$, $\mathbf{t}_{c2}$ and $\mathbf{t}_{s1}$, $\mathbf{t}_{s2}$ are the amplitude transmissions of the two AR coatings and the two substrates, respectively. To simplify the analysis, it is convenient to express these

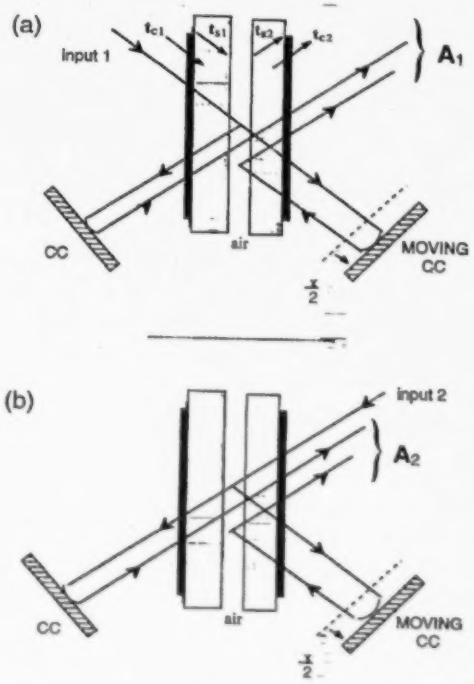

Fig. 8. Ray tracings showing the output amplitudes ($\mathbf{A}_1$ and $\mathbf{A}_2$) for (a) beams of unit amplitudes incident on input 1 and (b) input 2 for a beam splitter made of an optically thin layer of air squeezed between two substrates properly covered with AR coatings on their external faces.

amplitudes in terms of their respective modules and phases, yielding

$$\mathbf{t}_{s1} = t_{s1} \exp(i\sigma_1), \quad \mathbf{t}_{s2} = t_{s2} \exp(i\sigma_2),$$
$$\mathbf{t}_{c1} = t_{c1} \exp(i\Gamma_1), \quad \mathbf{t}_{c2} = t_{c2} \exp(i\Gamma_2). \quad \text{(A3)}$$

Use of these expressions in Eqs. (A1) and (A2) after rearrangement, leads to,

$$\mathbf{A}_1 = \mathbf{t}_{c1}\mathbf{t}_{s1}\mathbf{r}\mathbf{t}\mathbf{t}_{s2}\mathbf{t}_{c2}[t_{s1}{}^2t_{c1}{}^2 \exp(2i\sigma_1 + 2i\Gamma_1) + t_{s2}{}^2t_{c2}{}^2 \exp(2i\sigma_2 + 2i\Gamma_2)\exp(i\phi)] \quad \text{(A4)}$$

$$\mathbf{A}_2 = \mathbf{t}_{c2}{}^2\mathbf{t}_{s2}{}^2[\mathbf{t}^2t_{s1}{}^2t_{c1}{}^2 \exp(2i\sigma_1 + 2i\Gamma_1) + \mathbf{r}^2t_{s2}{}^2t_{c2}{}^2 \exp(2i\sigma_2 + 2i\Gamma_2)\exp(i\phi)]. \quad \text{(A5)}$$

The two output intensities I_1 and I_2 associated with each input port are found by multiplication of the two output amplitudes by their complex conjugates, which gives

$$I_1 = \mathbf{A}_1\mathbf{A}_1^* = T_{c1}T_{s1}R^2T_{s2}T_{c2}[H^2T_{s1}{}^2T_{c1}{}^2 + H^2T_{s2}{}^2T_{c2}{}^2 + H^2T_{s1}T_{c1}T_{s2}T_{c2}\cos(\phi + \psi)], \quad \text{(A6)}$$

$$I_2 = \mathbf{A}_2\mathbf{A}_2^* = R^2T_{s2}{}^2T_{c2}{}^2[H^4T_{s1}{}^2T_{c1}{}^2 + T_{s2}{}^2T_{c2}{}^2 + H^2T_{s1}T_{c1}T_{s2}T_{c2}\cos(\phi + \psi - \pi)], \quad \text{(A7)}$$

where a phase offset that is due to an imperfect compensation of the interferometer is defined as

$$\psi = 2(\sigma_2 + \Gamma_2 - \sigma_1 - \Gamma_1) \tag{A8}$$

and other quantities in uppercase letters are defined as follows:

$R = \mathbf{r}\mathbf{r}^*$, reflection in intensity of the thin layer of air;

$T_{s1} = \mathbf{t}_{s1}\mathbf{t}_{s1}^*$, transmission in intensity of substrate 1;

$T_{c1} = \mathbf{t}_{c1}\mathbf{t}_{c1}^*$, transmission in intensity of the AR coating onto substrate 1;

$T_{s2} = \mathbf{t}_{s2}\mathbf{t}_{s2}^*$, transmission in intensity of substrate 2;

$T_{c2} = \mathbf{t}_{c2}\mathbf{t}_{c2}^*$, transmission in intensity of the AR coating onto substrate 2.

Note that in Eqs. (A7) and (A8) the transmission in intensity of the thin layer of air does not appear explicitly but is defined as $T = RH^2$, where H is an intermediate variable such that

$$H = \frac{(1 - r_1^2)}{2r_1 \sin(\delta)} \tag{A9}$$

and where δ is the phase change of the beam on traversing the air layer. More information on how to derive H from Fresnel coefficients can be found in Ref. 21.

In Eqs. (A6) and (A7) the modulated components of the intensities represent the interferograms associated with each input port. It follows that the two complex responsivities $\mathbf{K}_1$ and $\mathbf{K}_2$ associated with each input are given by

$$\mathbf{K}_1 = K_1 \exp(i\psi) = +R^2H^2T_{s1}{}^2T_{c1}{}^2T_{s2}{}^2T_{c2}{}^2 \exp(i\psi), \tag{A10}$$

$$\mathbf{K}_2 = K_2 \exp[i(\psi - \pi)] = -R^2H^2T_{s1}T_{c1}T_{s2}{}^3T_{c2}{}^3 \exp(i\psi), \tag{A11}$$

which satisfies the balanced responsivities condition only when the two substrates and their AR coatings are optically identical, i.e., $T_{s1} = T_{s2}$ and $T_{c1} = T_{c2}$, yielding

$$\mathbf{K}_1 = -\mathbf{K}_2 = R^2H^2T_{s1}{}^4T_{c1}{}^4 \exp(i\psi). \tag{A12}$$

Note that to simplify the notation the contributions from other interferometer elements such as mirror reflections, window transmissions, detector responsivity, and electronics were not incorporated into the responsivity equations (A10) and (A11). However, this does not affect our conclusions, because if we assume a perfect optical symmetry between the two input components, it can be shown that these responsivity contributions from other components will affect both beam splitter responsivities [Eqs. (A10) and (A11)] by the same multiplicative factor, yielding no changes in relative terms, which is sufficient for the needs of the present modeling.

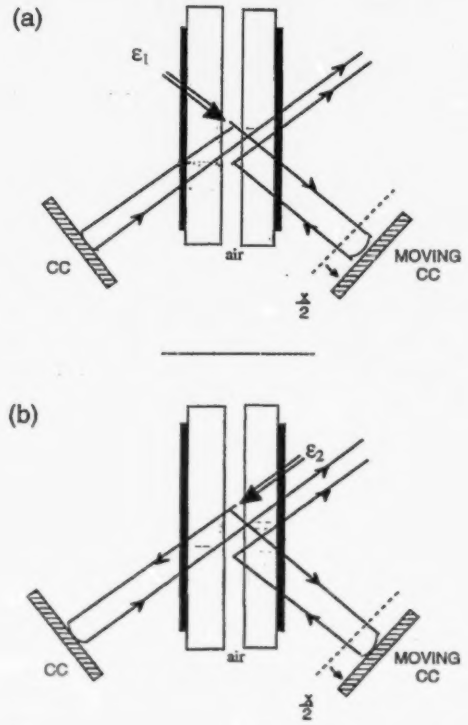

Fig. 9. Ray tracings representing the two internal emission components ε_1 and ε_2 from (a) substrate 1 and (b) substrate 2, respectively.

To evaluate the beam splitter self-emission, we use the parameters defined in Fig. 9, where

$$\varepsilon_1 = (1 - T_{c1}T_{s1})B_s, \tag{A13}$$

in which ε_1 represents the emission from substrate 1 incident on the thin air layer. Note that in Eq. (A13) the emission vanishes when both transmissions T_{c1} (AR coating) and T_{s1} (bulk substrate) are equal to one. When we use a ray tracing and a mathematical development similar to the one performed above, it can be shown that the modulated component of the interferogram associated with this substrate emission is given by

$$\text{modulation}(\varepsilon_1) = [(1 - T_{c1}T_{s1})B_s] \times R^2H^2T_{s1}T_{c1}T_{s2}{}^2T_{c2}{}^2 \cos(\phi + \psi), \tag{A14}$$

or, equivalently in the spectral domain, the corresponding raw spectrum associated with substrate-1 emission is given by

$$\text{raw spec}(\varepsilon_1) = \mathbf{K}_1 \frac{(1 - T_{c1}T_{s1})}{T_{c1}T_{s1}} B_s, \tag{A15}$$

where the complex responsivity $\mathbf{K}_1$ defined by Eq. (A10) is included in Eq. (A15). Similarly, the raw

spectrum associated with substrate-2 emission is given by

$$\text{raw spec}(\varepsilon_2) = \mathbf{K}_2 \frac{(1 - T_{c2}T_{s2})}{T_{c2}T_{s2}} B_s, \qquad \text{(A16)}$$

where the complex responsivity $\mathbf{K}_2$ is defined by Eq. (A11). Inspection of Eqs. (A15) and (A16) shows that the two emission spectra are 180° out of phase and cancel out when the two substrates and their corresponding AR coatings are optically identical, i.e., if $T_{s1} = T_{s2}$ and $T_{c1} = T_{c2}$, thus yielding

$$\text{raw spec}(\varepsilon_1) = -\text{raw spec}(\varepsilon_2). \qquad \text{(A17)}$$

Finally, it is important to note that Eqs. (A10), (A11), (A15), and (A16) are established for a single polarization axis (s or p) of the beam splitter. In principle, each polarization axis should be treated separately to obtain the corresponding responsivities and self-emissions. However, it can be shown that formally these equations also apply for the general case of mixed polarization (or unpolarized) provided that substrate transmissions and phases are redefined by effective quantities. An effect of this can be seen in the spectral region where the two beam splitter substrates absorb differently (see Fig. 3 between 550 and 700 cm^{-1}). In this case the effective phase difference between the two responsivities could be other than the 180° predicted by Eq. (A12). This can be understood from Fresnel coefficients,[22] which shows that the phase shifts at the interface of an absorbing medium are different for each polarization. Consequently, the effective responsivities (mixed polarization) for input 1 and input 2 can have a phase difference other than 180°. Note that for the interface of a transparent medium the phase shift is the same for the two polarizations, yielding an effective phase difference of 180° for this particular case (see Fig. 3 above 800 cm^{-1}).

The author thanks Luc Bissonnette for many helpful suggestions related to this study. The technical assistance of Claude Bradette throughout this study is gratefully acknowledged. Special thanks to Martin Chamberland, Jean Giroux, and Jacques McKinnon from Bomem for their expert contributions to developing the CATSI concept and to building the system.

References and Notes

1. W. L. Smith, H. M. Woolf, and H. E. Revercomb, "Linear simultaneous solution for the retrieval of temperature and absorbing constituents from radiance spectra," Appl. Opt. **30**, 1117–1123 (1991).
2. D. Lubin and A. S. Simpson, "The Longwave emission signature of urban pollution: radiometric FTIR measurement," Geophys. Res. Lett. **21**, 37–40 (1994).
3. W. F. J. Evans and E. Puckrin, "An observation of the atmospheric emission spectrum of CFC-11," Geophys. Res. Lett. **21**, 2381–2384 (1994).
4. M. L. Polak, J. L. Hall, and K. C. Herr, "Passive Fourier-transform infrared spectroscopy of chemical plumes: an algorithm for quantitative interpretation and real-time background removal," Appl. Opt. **34**, 5406–5412 (1995).
5. R. T. Kroutil, R. J. Combs, R. B. Knapp, and J. P. Godfrey, "Infrared interferogram analysis for ammonia detection with passive FT-IR spectrometry," in *Electro-Optical Technology for Remote Chemical Detection and Identification*, M. Fallahi and E. Howden, eds., Proc. SPIE **2763**, 86–102 (1996).
6. D. S. Flanigan, "Prediction of the limits of detection of hazardous vapors by passive infrared with the use of MODTRAN," Appl. Opt. **35**, 6090–6098 (1996).
7. R. V. Allen, F. J. Mucray, and X. Liu, "Mid-infrared measurements of the atmospheric emission over the South Pole using a radiometrically calibrated Fourier transform Spectrometer," Appl. Opt. **35**, 1523–1530 (1996).
8. J.-M. Thériault, C. Bradette, and J. Gilbert, "Atmospheric remote sensing with a ground-based spectrometer system," in *Infrared Technology and Applications XXII*, B. F. Andresen, M. Strojnik, and M. S. Scholl, eds., Proc. SPIE **2744**, 664–672 (1996).
9. Also see recent papers in Proceedings of the SPIE Conference on Electro-Optical Technology for Remote Chemical Detection and Identification, M. Fallahi and E. Howden, eds., Proc. SPIE **2763** (1996), Proc. SPIE **3082** (1997), Proc. SPIE **3383** (1998).
10. J.-M. Thériault, C. Bradette, A. Villemaire, M. Chamberland, and J. Giroux, "Differential detection with a double-beam interferometer," in *Electro-Optical Technology for Remote Chemical Detection and Identification II*, M. Fallahi and E. Howden, eds., Proc. SPIE **3082**, 65–75 (1997).
11. A. Villemaire, M. Chamberland, J. Giroux, R. L. Lachance, and J.-M. Thériault, "Radiometric calibration of FT-IR remote sensing instrument," in *Electro-Optical Technology for Remote Chemical Detection and Identification II*, M. Fallahi and E. Howden, eds., Proc. SPIE **3082**, 83–91 (1997).
12. R. L. Lachance, J.-M. Thériault, C. Lafond, and A. Villemaire, "Gaseous emanation detection algorithm using a Fourier transform interferometer operating in differential mode," in *Electro-Optical Technology for Remote Chemical Detection and Identification III*, M. Fallahi and E. Howden, eds., Proc. SPIE **3383**, 124–132 (1998).
13. P. Fellgett, "Les progrès Récents en spectroscopie interférentielle, Bellevue," Colloq. Int. C. N. R. S. p. 53 (1957).
14. T. F. Zehnpfennig, O. Shepherd, S. Rappaport, W. P. Reidy, and G. Vanasse, "Background suppression in double-beam interferometry," Appl. Opt. **18**, 1996–2002 (1979).
15. G. A. Vanasse, R. E. Murphy, and F. H. Cook, "Double-beaming technique in Fourier spectroscopy," Appl. Opt. **15**, 290–291 (1976).
16. O. Shepherd, A. G. Hurd, R. B. Wattson, H. J. P. Smith, and G. A. Vanasse, "Spectral measurements of stack effluents using a double-beam interferometer with background suppression," Appl. Opt. **20**, 3972–3980 (1981).
17. H. Krenn, I. Roschger, and G. Bauer, "Dual-beam interferometer for optical difference measurements," Appl. Opt. **23**, 3065–3074 (1984).
18. H. E. Revercomb, H. Buijs, H. B. Howell, D. D. Laporte, W. L. Smith, and L. A. Sromovsky, "Radiometric calibration of IR Fourier transform spectrometers: solution to a problem with the high-resolution interferometer sounder," Appl. Opt. **27**, 3210–3218 (1988).
19. C. Weddigen, C. E. Blom, and M. Höpfner, "Phase corrections for the emission sounder MIPAS-FT," Appl. Opt. **32**, 4586–4589 (1993).
20. J. Schreiber, T. Blumenstock, and H. Ficher, "Effects of the self-emission of an IR Fourier-transform spectrometer on measured absorption spectra," Appl. Opt. **35**, 6203–6209 (1996).
21. J.-M. Thériault, "Beam splitter layer emission in Fourier-transform infrared Interferometer," Appl. Opt. **37**, 8348–8351 (1998).
22. O. S. Heavens, *Optical Properties of Thin Solid Films* (Dover, New York, 1965).